Decentralized Model Predictive Control for Equilibrium-based Collaborative UAV Bar Transportation

Roberto C. Sundin[†], Pedro Roque[‡], and Dimos V. Dimarogonas[‡]

***Abstract*— In this paper we analyze the equilibrium points of a collaborative transportation task, composed of two unmanned aerial vehicles and a payload - in this case, a bar. Moreover, centralized and decentralized linear model predictive controllers are designed, where the nonlinear dynamics are linearized around the equilibrium points previously analyzed. A comparison between the centralized and decentralized formulations is provided, based on experimental results for both setups, and considering the time to solution and performance of each controller. Our findings provide new operational equilibrium points that can be paired with predictive model-based controllers for efficient operation.**

I. INTRODUCTION

The maneuverability and freedom provided by unmanned aerial vehicles (UAVs) are useful in a variety of applications. UAVs have already been used in search and rescue missions [1], and in inspection and defect detection of solar panels, bridges and building facades [2]–[4]. Another use case for UAVs is payload transport. However, the geometry and weight of the payload may often require the use of more than one UAV to make transport possible, creating a need for a controller structure with multi-agent capabilities. Furthermore, the geometric constraints introduced by the coupling between UAVs and payload, often result in complex dynamics with intricate interaction forces, rendering the control problem far from straightforward.

A common denominator for much of the previous work on UAV payload transport is to either treat the payload as a disturbance, or to find workarounds to bypass the need for modeling its complete dynamics. In [5], robust MPC with a disturbance term to account for the unknown dynamics of the load is used, and therefore cannot offer optimality with respect to its dynamics. In [6], a UAV–bar system (similar to fig. 1) is approximated by two UAVs with separate point-mass payloads, where each of the agents is controlled with an LQR. Other approaches take into account the full dynamics of the payload: in [7], [8] the authors design appropriate PID-based control laws to stabilize the UAV–bar system, accounting for a single equilibrium point; in [9], an offline batch optimization routine taking into account the string tension forces is used to generate appropriate trajectories. These approaches, however, lack look-ahead capabilities or online-feedback, leading to non-optimal control inputs. Lastly, in [10], open-loop control forces are designed as a function of the object's internal forces, given by end-effector sensor readings. As these are open-loop forces, steady-state error is present when no internal forces are measured.

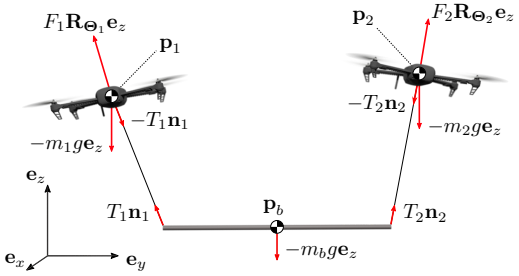

Fig. 1: The system under analysis in this work, where two UAVs collaboratively transport a bar using cables.

In this work we propose Model Predictive Controllers (MPCs) to control the UAV–bar system depicted in Fig. 1. In this scenario, two UAVs collaboratively transport a cylindrical payload and two MPC control methodologies are tested: one centralized, and one decentralized. The centralized controller bears resemblance to the one found in [11], but instead of performing a numerical linearization step online, the linearization is done analytically as part of the modeling process, saving valuable computational time. The contributions are threefold: i) an analysis of the equilibrium points of the system depicted in Fig. 1 is provided, leading to an efficient formulation capable of being used in an online MPC framework; ii) experimental results that showcase both the centralized and decentralized control methodologies, based on the equilibrium analysis results; iii) a comparative of the results, particularly highlighting the differences between the two control setups.

Notation: Small, bold letters represent vectors. Matrices are denoted by bold, capital letters. Regular letters denote scalars. ${}_\times\mathbf{a}$ denotes the skew-symmetric matrix representation of $\mathbf{a}$, and $\mathbf{a}^T$ the transpose of $\mathbf{a}$. Calligraphic letters denote reference frames, and the basis vectors of a frame $\mathcal{A}$ are denoted $\{\mathbf{a}_x, \mathbf{a}_y, \mathbf{a}_z\}$. We denote by $\mathbf{0}_N \in \mathbb{R}^N$ the column vector of all zeros. Rotation matrices from frames $\mathcal{A}$ to $\mathcal{B}$ are defined as $\mathbf{R}_{\mathcal{A}/\mathcal{B}} \in \mathcal{SO}(3)$. Features represented in a reference frame $\mathcal{A}$ are denoted as ${}^{\mathcal{A}}\mathbf{a}$. When the origin/target frame is the inertial frame, we omit the corresponding letter. Sets are defined using capital sans-serif letters, *e.g.*, A. The weighted vector norm $\sqrt{\mathbf{x}^T\mathbf{A}\mathbf{x}}$ is denoted $\|\mathbf{x}\|_{\mathbf{A}}$. The

[†]Roberto C. Sundin is with Ericsson Research, Stockholm, Sweden. E-Mail: roberto.castro.sundin@ericsson.com

[‡]P. Roque and D. V. Dimarogonas are with the Division of Decision and Control Systems, KTH Royal Institute of Technology, Stockholm, Sweden. E-Mail: {padr, dimos}@kth.se

This work was supported by the H2020 ERC Grant LEAFHOUND, the Swedish Foundation for Strategic Research (SSF), the Swedish Research Council (VR) and the Knut och Alice Wallenberg Foundation (KAW).

indexed letters $s_{(\cdot)}$, $c_{(\cdot)}$, and $t_{(\cdot)}$ denote the trigonometric functions $\sin(\cdot)$, $\cos(\cdot)$, and $\tan(\cdot)$, respectively.

II. BACKGROUND

In this section we provide the necessary background knowledge for the paper.

A. UAV with Single Load

Let $\{\mathcal{E}\}$ and $\{\mathcal{B}\}$ denote an inertial frame, and UAV body frame, respectively, where the frame $\{\mathcal{B}\}$ is attached and kept fixed to the UAV center of mass (CoM) as in Fig. 2. Let the positions $\mathbf{p}$ and $\mathbf{p}_p$, the velocities $\mathbf{v}$ and $\mathbf{v}_p$, and the masses m and m_p, correspond to those of the UAV and the payload, respectively. Moreover, let g be the gravity constant, $\mathbf{\Theta}$ be the Euler angles of the UAV body w.r.t. $\{\mathcal{E}\}$, $\mathbf{J}$ its positive definite inertia matrix and $\boldsymbol{\omega}_{\mathcal{B}}$ its body angular rates. Although the forces and moments that the UAV is able to generate are effects of the combination of the thrusts generated by each propeller, a frequently used technique is to combine these thrusts into a single thrust (here F_t), and a torque vector (here $\boldsymbol{\tau}_{\mathcal{B}}$) [12], [13]. This technique is motivated by that each pair $(F_t, \boldsymbol{\tau}_{\mathcal{B}})$, uniquely defines the thrust of each propeller [13]. Then, the equations of motion of the UAV-payload system can be found using the Newton-Euler approach, resulting in

$$\dot{\mathbf{p}} = \mathbf{v} \tag{1a}$$
$$\dot{\mathbf{v}} = m^{-1}(F_t\mathbf{R}\mathbf{e}_z - mg\mathbf{e}_z - T\mathbf{n}) \tag{1b}$$
$$\dot{\mathbf{\Theta}} = \mathbf{H}\,{}^{\mathcal{B}}\boldsymbol{\omega}, \tag{1c}$$
$${}^{\mathcal{B}}\dot{\boldsymbol{\omega}} = \mathbf{J}^{-1}\left({}^{\mathcal{B}}\boldsymbol{\tau} - {}^{\mathcal{B}}_{\times}\boldsymbol{\omega}\mathbf{J}\,{}^{\mathcal{B}}\boldsymbol{\omega}\right) \tag{1d}$$
$$\dot{\mathbf{p}}_p = \mathbf{v}_p \tag{1e}$$
$$\dot{\mathbf{v}}_p = m_p^{-1}\left(T\mathbf{n} - m_p g\mathbf{e}_z\right) \tag{1f}$$

where l is the cable length, $\mathbf{n} = l^{-1}(\mathbf{p} - \mathbf{p}_p)$ is the cable direction vector, $\mathbf{R}$ is the Z-Y-X Rotation matrix, T is the absolute tension force in the cable attached to the payload [14, eq. (5)] and $\mathbf{H}$ the attitude Jacobian that translates body rates to Euler angles [15]. These are given by

$$\mathbf{R}(\phi,\theta,\psi) = \begin{bmatrix} c_\psi c_\theta & c_\psi s_\theta s_\phi - s_\psi c_\phi & c_\psi s_\theta c_\phi + s_\psi s_\phi \\ s_\psi c_\theta & s_\psi s_\theta s_\phi + c_\psi c_\phi & s_\psi s_\theta c_\phi - c_\psi s_\phi \\ -s_\theta & c_\theta s_\phi & c_\theta c_\phi \end{bmatrix}, \tag{2}$$

$$T = m_p(m_p+m)^{-1}\left(F_t\mathbf{R}\mathbf{e}_z\cdot\mathbf{n} + ml^{-1}\|\mathbf{v}-\mathbf{v}_p\|^2\right), \tag{3}$$

$$\mathbf{H} = \begin{bmatrix} 1 & s_\phi t_\theta & c_\phi t_\theta \\ 0 & c_\phi & -s_\phi \\ 0 & s_\phi/c_\theta & c_\phi/c_\theta \end{bmatrix}, \tag{4}$$

where the angles ϕ, θ, and ψ are referred to as roll, pitch, and yaw, respectively.

B. UAVs with bar

We now consider a system where a rigid bar is tethered to two UAVs by cables, as illustrated in Fig. 1. Each UAV is given a corresponding body frame $\{\mathcal{B}_i\}$, $i = 1, 2$, that is attached to the UAV CoM, and to where it is assumed that the cables are attached. The bar, however, is chosen to be modeled solely with respect to the inertial frame $\{\mathcal{E}\}$. The

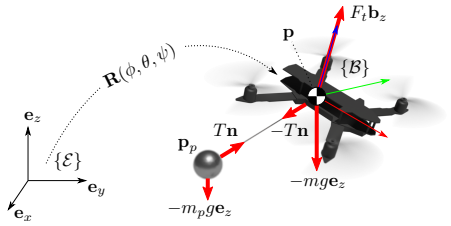

Fig. 2: A UAV with payload attached, and an associated body frame $\{\mathcal{B}\}$ located at a position $\mathbf{p}$ with respect to the inertial frame $\{\mathcal{E}\}$.

state variables introduced in the previous section are also given subindices, so that, *e.g.*, $\mathbf{p}_1$ is the position of UAV 1. The subindex b is used for quantities relating to the bar.

Each cable is of length l_1 and l_2, respectively, where the subindex is given depending on to which UAV the cable is directly attached to. We denote by m_b the mass of the bar, and d_i the distance between the bar CoM and the end of the bar to which cable i is attached. Thus, the total length of the bar is (d_1+d_2). Furthermore we define $\mathbf{n}_b$ as the unit vector parallel with the bar's symmetry axis, pointing towards the attachment of cable 2. Each cable direction is, in this case, given by $\mathbf{n}_i = l_i^{-1}(\mathbf{p}_i - (\mathbf{p}_b + (-1)^i d_i\mathbf{n}_b))$, $i = 1, 2$.

Using the same Newton-Euler approach as for the single UAV case results in the following set of equations

$$\dot{\mathbf{p}}_i = \mathbf{v}_i \qquad i = 1,2,b \tag{5a}$$
$$\dot{\mathbf{v}}_i = m_i^{-1}\left(F_i\mathbf{R}_{\mathbf{\Theta}_i}\mathbf{e}_z - m_i g\mathbf{e}_z - T_i\mathbf{n}_i\right) \quad i = 1,2 \tag{5b}$$
$$\dot{\mathbf{\Theta}}_i = \mathbf{H}_{\mathbf{\Theta}_i}\,{}^{\mathcal{B}}\boldsymbol{\omega}_i \quad i = 1,2 \tag{5c}$$
$${}^{\mathcal{B}}\dot{\boldsymbol{\omega}}_i = \mathbf{J}_i^{-1}\left({}^{\mathcal{B}}\boldsymbol{\tau}_i - {}^{\mathcal{B}}_{\times}\boldsymbol{\omega}_i\mathbf{J}_i\,{}^{\mathcal{B}}\boldsymbol{\omega}_i\right) \quad i = 1,2 \tag{5d}$$
$$\dot{\mathbf{v}}_b = m_b^{-1}(T_1\mathbf{n}_1 + T_2\mathbf{n}_2 - m_b g\mathbf{e}_z) \tag{5e}$$
$$\dot{\mathbf{\Theta}}_b = \mathbf{H}^{\{\mathcal{E}\}}_{\mathbf{\Theta}_b}\boldsymbol{\omega}_b \tag{5f}$$
$$\dot{\boldsymbol{\omega}}_b = J_b^{-1}\,{}_{\times}\mathbf{n}_b(d_2T_2\mathbf{n}_2 - d_1T_1\mathbf{n}_1) \tag{5g}$$

where $\mathbf{R}_{\mathbf{\Theta}_i}$, $\mathbf{H}_{\mathbf{\Theta}_i}$ are found by making the substitutions $\phi \leftarrow \phi_i$, $\theta \leftarrow \theta_i$, and $\psi \leftarrow \psi_i$ in (2) and (4), respectively. The matrix $\mathbf{H}^{\{\mathcal{E}\}}_{\mathbf{\Theta}_b}$, relates angular velocities in the *inertial* frame to Euler-angle rates and has the form

$$\mathbf{H}^{\{\mathcal{E}\}}_{\mathbf{\Theta}_b} = \begin{bmatrix} c_{\psi_b}/c_{\theta_b} & s_{\psi_b}/c_{\theta_b} & 0 \\ -s_{\psi_b} & c_{\psi_b} & 0 \\ c_{\psi_b}t_{\theta_b} & s_{\psi_b}t_{\theta_b} & 1 \end{bmatrix}. \tag{6}$$

Equation (5g) is valid under the assumption that $\mathbf{n}_b\cdot\boldsymbol{\omega}_b = 0$, and J_b can in this case be chosen to be the scalar corresponding to the moment of inertia in the axes perpendicular to $\mathbf{n}_b$.

To reduce the model complexity, each cable is modeled as a massless, rigid, and rotational link, which means that the following constraint

$$\left\|\mathbf{p}_i - (\mathbf{p}_b + (-1)^i d_i\mathbf{n}_b)\right\| = l_i, \qquad i = 1,2 \tag{7}$$

holds, and the forces T_1, T_2 take the form

$$\begin{bmatrix} T_1 \\ T_2 \end{bmatrix} = \mathbf{M}^{-1}\boldsymbol{\lambda}, \tag{8}$$

for a matrix $\mathbf{M} \in \mathbb{R}^{2\times 2}$, and a vector $\boldsymbol{\lambda} \in \mathbb{R}^2$, both being functions of the state and input. For an explicit expression, see [16].

Fig. 3: Definition of the angles θ_f and θ_l. The system is assumed symmetric with respect to the center of the bar. The variable θ_l corresponds to the angle between the cable and inertial Z-axis, while θ_f corresponds to the angle between the thrust F_i being applied on the cable and the inertial Z-axis.

III. Equilibrium points for the UAV–bar system

A result of this work corresponds to the analysis of the equilibrium points of the system depicted in Fig. 1.

Assumption 1. *Consider the system* (5)*, where the variables* T_1 *and* T_2 *are defined according to* (8)*. It is assumed that the system is symmetric with* $d_1 = d_2 =: d_b$*,* $l_1 = l_2 =: l$*, and* $m_1 = m_2 =: m_{\text{uav}}$*. It is also assumed that the bar is parallel with* $\mathbf{e}_x$*, and that it is placed with its center of mass in the origin.*

Under these conditions, it is possible to obtain a set of equilibrium points, as shown in Proposition 1.

Proposition 1. *Let Assumption 1 hold. Then the equilibrium points of* (5) *can be defined in closed form with respect to* θ_f *and* θ_l*, where* θ_l *corresponds to the angle between the cable and inertial Z-axis and* θ_f *corresponds to the angle between the thrust* F_i *being applied on the cable and the inertial Z-axis, according to* $f_{\text{eq}}(\theta_f, \theta_l) = 0$*, where*

$$f_{\text{eq}}(\theta_f,\theta_l) = \left(\frac{s_{\theta_f} M g}{2c_{\theta_f}} - \frac{m_b g c_{(\theta_f-\theta_l)} s_{\theta_l} M}{2c_{\theta_f}\left(2m_{\text{uav}} {c_{\theta_l}}^2 + m_b\right)}\right)^2 + \\ + \left(\frac{m_b g}{2} - \frac{m_b g c_{(\theta_f-\theta_l)} c_{\theta_l} M}{2c_{\theta_f}\left(2m_{\text{uav}} {c_{\theta_l}}^2 + m_b\right)}\right)^2, \tag{9}$$

with $M := m_b + 2m_{\text{uav}}$.

Proof. Consider the parametrization variables θ_f and θ_l as in Fig. 3, the thrust forces as $\mathbf{f}_i = F \cdot (\sin\theta_f \cdot (-1)^i, 0, \cos\theta_f)$, $i = 1, 2$, and the string tension forces as $\mathbf{t}_i = T \cdot (\sin\theta_l \cdot (-1)^i, 0, \cos\theta_l)$, $i = 1, 2$. This restricts the UAV positions, so that $\mathbf{p}_i = ((d_b + l\sin\theta_l)\cdot(-1)^i, 0, \cos\theta_l)$, $i = 1, 2$. For the vertical equilibrium of the system, we need $(\mathbf{f}_1 + \mathbf{f}_2)\cdot\mathbf{e}_z = 2F\cos\theta_f = g(m_b + 2m_{\text{uav}})$, which gives

$$F = gM(2\cos\theta_f)^{-1} \tag{10}$$

Similarly, for the lateral equilibrium $(\mathbf{f}_i - \mathbf{t}_i)\cdot\mathbf{e}_x = 0$, $i = 1, 2$, must hold, but the symmetry given by Assumption 1 and the definition of θ_f, θ_l implies that this can be reduced to the single equation

$$F\sin\theta_f - T\sin\theta_l = 0. \tag{11}$$

The string tension force T can be taken from (8) (by symmetry, $T_1 = T_2$), giving $T = \frac{m_b g\cos(\theta_f-\theta_l)(m_b+2m_{\text{uav}})}{2\cos(\theta_f)(2m_{\text{uav}}\cos^2(\theta_l)+m_b)}$ after substituting F using (10). Finally for the bar to be in equilibrium, it is necessary that the string tensions' vertical components are equal to the weight of the bar, *i.e.*,

$$T\cos\theta_l - \frac{m_b g}{2} = 0. \tag{12}$$

Note that, the lateral equilibrium is fulfilled automatically due to symmetry. The result now follows from the squared sum of (11) and (12), giving $f_{\text{eq}}(\theta_f, \theta_l) = 0$. □

Out of all solutions, the trivial solution $\theta_f = \theta_l = 0$ constitutes the most efficient equilibrium point as the thrust direction is then completely aligned with the direction of gravity. The other equilibria, however, remain interesting in situations where the space in the z-direction is limited, and also enables the possibility of raising the bar while the z-position of the UAVs remains relatively intact (or lowering the UAVs while the bar remains in position.)

IV. Centralized controller

This controller makes use of the model derived in Section II-B. To reduce the system complexity and consequently the MPC solving time we make use of a linearized version of (5), leaving the yaw of each rigid body as a parameter that is set at each sampling time. As linearization point, any of the equilibria defined by the solution to (9) can be chosen, as long as Assumption 1 holds. While the bar can assume an arbitrary position $\mathbf{p}_b$, the positions of the UAVs are decided explicitly based on the yaw and the position of the bar if the system is to remain in the chosen equilibrium position. Consequently, the equilibrium state is given by $\mathbf{x}_{\text{eq}} = (\mathbf{x}_{\text{eq}}^{(b)}, \mathbf{x}_{\text{eq}}^{(1)}, \mathbf{x}_{\text{eq}}^{(2)})$, where $\mathbf{x}_{\text{eq}}^{(b)} = (\mathbf{p}_b, \mathbf{0}_5, \psi_0^{(b)}, \mathbf{0}_3)$, $\mathbf{x}_{\text{eq}}^{(i)} = (\mathbf{p}_i, \mathbf{0}_4, (-1)^{i-1}\theta_f, \psi_0^{(i)}, \mathbf{0}_3)$, $i = 1, 2$, and $\mathbf{p}_i = \mathbf{p}_b + ((-1)^{i-1}(d_i + l_i s_{\theta_l})\sin\psi_0^{(b)}, (-1)^i(d_i + l_i s_{\theta_l})\cos\psi_0^{(b)}, l_i c_{\theta_l})$, $i = 1, 2$. The corresponding input equilibrium is given by the conditions of force and moment equilibria which result in $\mathbf{u}_{\text{eq}} = (F_{\text{eq}}^{(1)}, {}^{\mathcal{B}}\boldsymbol{\tau}_{\text{eq}}^{(1)}, F_{\text{eq}}^{(2)}, {}^{\mathcal{B}}\boldsymbol{\tau}_{\text{eq}}^{(2)})$, where ${}^{\mathcal{B}}\boldsymbol{\tau}_{\text{eq}}^{(1)} = {}^{\mathcal{B}}\boldsymbol{\tau}_{\text{eq}}^{(2)} = \mathbf{0}_3$, and $F_{\text{eq}}^{(i)} = gM/(2c_{\theta_f})$. The resulting linearized system equations can be written as $\dot{\mathbf{x}}_{\text{lin}}(t) := \mathbf{A}_c\Delta\mathbf{x}(t) + \mathbf{B}_c\Delta\mathbf{u}(t)$, where $\mathbf{A}_c = \partial\dot{\mathbf{x}}/\partial\mathbf{x}\,\big|_{\mathbf{x}=\mathbf{x}_{\text{eq}}}$, $\mathbf{B}_c = \partial\dot{\mathbf{x}}/\partial\mathbf{u}\,\big|_{\mathbf{x}=\mathbf{x}_{\text{eq}}}$, $\Delta\mathbf{x} := \mathbf{x} - \mathbf{x}_{\text{eq}}$, and $\Delta\mathbf{u} := \mathbf{u} - \mathbf{u}_{\text{eq}}$. The standard zero-order hold (ZOH) discretization of $\dot{\mathbf{x}}_{\text{lin}}$ would result in many higher order terms of the parameters $\psi_0^{(b)}$, $\psi_0^{(1)}$, and $\psi_0^{(2)}$, and we therefore use a first order approximation $\mathbf{x}[k+1] = \mathbf{A}\Delta\mathbf{x}[k] + \mathbf{B}\Delta\mathbf{u}[k]$, where $\mathbf{A} = \mathbf{I} + \mathbf{A}_c h$, $\mathbf{B} = \mathbf{B}_c h$, and h is the sampling time.

Finally the MPC optimization problem is given by

$$\begin{aligned} \min_{\{\mathbf{u}[i]\}_{i=0}^{N-1}} \quad & \sum_{k=0}^{N-1}\left(\|\Delta\mathbf{x}[k]\|_{\mathbf{Q}}^2 + \|\Delta\mathbf{u}[k]\|_{\mathbf{R}_{\text{MPC}}}^2\right) \\ & + \|\Delta\mathbf{x}[N]\|_{\mathbf{Q}_N}^2 \\ \text{s.t.} \quad & \mathbf{x}[k+1] = \mathbf{A}\mathbf{x}[k] + \mathbf{B}\mathbf{u}[k], \qquad \text{(MPC)} \\ & \mathbf{x}[k] \in \mathsf{X}, \quad k = 0, \ldots, N-1, \\ & \mathbf{u}[k] \in \mathsf{U}, \quad k = 0, \ldots, N-1, \\ & \mathbf{x}[N] \in \mathsf{X}_N, \\ & \mathbf{x}[0] := \mathbf{x}(t_s) \end{aligned}$$

for each sampling time t_s, and where the full state vector $\mathbf{x} \in \mathbb{R}^{36}$ is ordered $\mathbf{x} = (\mathbf{p}_b, \mathbf{v}_b, \boldsymbol{\Theta}_b, \boldsymbol{\omega}_b, \mathbf{p}_1, \mathbf{v}_1, \boldsymbol{\Theta}_1, \boldsymbol{\omega}_1, \mathbf{p}_2, \mathbf{v}_2, \boldsymbol{\Theta}_2, \boldsymbol{\omega}_2)$, the

matrices $\mathbf{Q}$, $\mathbf{Q}_N$, $\mathbf{R}_{\text{MPC}}$ are user-designed positive definite weighting matrices, and the constraint sets X, X_N, U define the state, terminal state and control input constraints. The solution to (MPC) will be a set of vectors $\{\mathbf{u}[i]\}_{i=0}^{N-1}$, out of which only the first, $\mathbf{u}[0] =: \mathbf{u}^*$, will be applied.

V. DECENTRALIZED CONTROLLER

In this section, we aim to decentralize the controller structure defined in the previous section. While there could be many benefits of a decentralization, the main point of interest within this work is to investigate how this decentralization affects the MPC solving time and the overall performance of the closed-loop system.

Since the UAVs are dynamically coupled by the cable tension force T, the original system cannot be decentralized without modifications. For this reason, the UAV–bar system is approximated further by instead considering it as two independent UAVs with payloads. Hence, the endpoints of the bar are tracked, and their position and velocity considered as the positions and velocities of imaginary payloads attached to each UAV by cables. The weight given to each (imaginary) payload is set to the same weight the bar would apply to the cable in the U-shaped equilibrium pose where $\mathbf{n}_1 = \mathbf{n}_2 = \mathbf{e}_z$ and $\mathbf{n}_b \cdot \mathbf{e}_z = 0$, which would be equal to $m_b/2$ in a symmetric setup, but more generally

$$m_p^{(i)} := m_b d_i^{-1}(d_1 + d_2)^{-1} d_2 d_1, \tag{13}$$

Using the model description in Section II-A, the model used in the controller of UAV i is then found by updating m_p using (13) in (1f) and (3), followed by a linearization and discretization as explained in Section IV. Once the models are derived, an MPC can be designed for each UAV as in (MPC). In other words, each UAV (with payload) defines its own MPC optimization problem, each of which can be solved independently, making this a decentralized setup. We have chosen the ordering of the state vector of UAV i, $\mathbf{x}_i \in \mathbb{R}^{18}$, as $\mathbf{x}_i = (\mathbf{p}_i, \mathbf{v}_i, \boldsymbol{\Theta}_i, \boldsymbol{\omega}_i, \mathbf{p}_p, \mathbf{v}_p)$.

VI. EXPERIMENTAL SETUP

Two Storm SRD370 quadrotors equipped with onboard mRo Pixracer flight control units (FCUs) flashed with PX4 firmware version `1.10.1`, were connected with a host computer (Intel i7-6700@3.4GHz, 8 threads; 32 GB DDR4@2133 MHz) over Wi-Fi and communicated using the `MAVLink` (`https://mavlink.io`) messaging protocol. The host computer used `MAVLink` accompanied with `MAVROS`, which enabled the translation of Robot Operating System (ROS) messages to the relevant `MAVLink` messages. A motion capture system (Qualisys) was used for receiving state estimates. Fig. 4 provides a schematic of the network.

Both MPCs were implemented as a ROS node and the optimal control problems formulated in `CasADi` [17] and solved using the `HPMPC` solver. The parameters of the centralized MPC were set as seen in Table I, and the decentralized MPC as in Table II for both UAVs. For both controllers the input constraints U were set in order to guarantee a

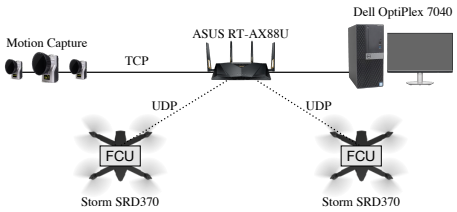

Fig. 4: An illustration of the experimental setup where solid (dashed) lines represent wired (wireless) connections.

TABLE I: Parameter settings the centralized MPC.

$\mathbf{Q}$	$\text{diag}(\mathbf{Q}'_b, \mathbf{Q}'_{\text{UAVs}}, \mathbf{Q}'_{\text{UAVs}})$
$\mathbf{Q}'_b$	$\text{diag}(50, 50, 50, 50, 50, 50, 10, 10, 10, 1, 1, 5)$
$\mathbf{Q}'_{\text{UAVs}}$	$\text{diag}(30, 30, 30, 30, 30, 30, 10, 10, 20, 10, 10, 100)$
$\mathbf{R}_{\text{MPC}}$	$\text{diag}(1, 100, 100, 50, 1, 100, 100, 50)$
$\mathbf{Q}_N$	$100\mathbf{Q}$
h	0.02 s
N	30

positive thrust ($F_i > 0$) and such that the torque magnitudes were less than or equal to one ($\|\boldsymbol{\tau}_{\mathcal{B},i}\|_\infty \leq 1\,\text{N m}$). Initial benchmarks of the CPU time required by the MPCs, gave results averaging sligthly below 10 ms, and thus the sampling time h was set to 20 ms to allow for occasional CPU time increases.

The experiments were performed at the $6 \times 6 \times 3\,\text{m}^3$ arena at the KTH Smart Mobility Lab, where both controllers were setup to track four setpoints in sequence. As payload, a hollow bar weighing 0.39 kg and of length 1.47 m was used, and the Storm SRD370s were modeled as having masses $m_i = 1.15\,\text{kg}$, and moments of inertia $\mathbf{J}_i = \text{diag}(0.0348, 0.0459, 0.0977)\,\text{kg m}^2$. During initial tests of the decentralized MPC setup it was discovered that the assumption that the bar was homogenous with a CoM in the center of its extension along the axis of symmetry was not accurate enough. Instead, d_1 and d_2 were re-identified and found to be $d_1 = 70.5\,\text{cm}$ and $d_2 = 76.5\,\text{cm}$, and the values of $m_p^{(i)}$ were updated according to (13).

VII. RESULTS

In this section we analyze the results obtained by implementing the controllers in Sections IV and V to a real system. An accompanying video showcases the experiments. Before setting up the experimental platform, both controllers were tested in a `Gazebo` simulation environment running the PX4 software in the loop (SITL) using the following setpoints (fig. 5): first the bar is rotated 90 degrees around its centerpoint, while UAV 1 also rotates an equal amount. Then the bar is translated a distance of one meter while

TABLE II: Parameter settings for the decentralized MPCs.

$\mathbf{Q}$	$\text{diag}(\mathbf{Q}'_{\text{UAV}}, \mathbf{Q}'_p)$
$\mathbf{Q}'_{\text{UAVs}}$	$\text{diag}(20, 20, 20, 30, 30, 30, 10, 10, 30, 10, 10, 30)$
$\mathbf{Q}'_p$	$\text{diag}(20, 20, 20, 1, 1, 1)$
$\mathbf{R}_{\text{MPC}}$	$\text{diag}(1, 100, 100, 100)$
$\mathbf{Q}_N$	$50\mathbf{Q}$
h	0.02 s
N	30

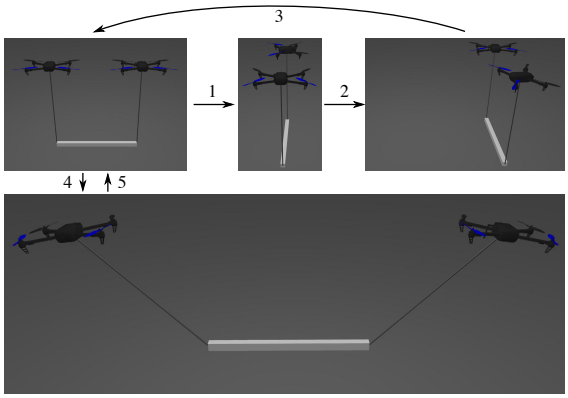

Fig. 5: Images of the setpoints used in a preliminary simulation using the PX4 SITL.

both UAVs rotate 90 degrees. After returning back to the original position, the system is then set to the equilibrium point described by $\theta_f = 0.1183$, $\theta_l = \pi/4$ (this is a solution to (9) for $m_{\text{uav}} = 1.52$ kg, $m_b = 0.41$ kg, and $g = 9.81$ m/s^2) before finally assuming the initial configuration.

A. Centralized MPC

Figs. 6a and 6b show the position and orientation of all rigid bodies, as well as the reference signals (in dashed lines). Figs. 7a and 7b show the resulting optimal control signals. The overall behaviour of the controller is consistent with initial simulation results (left out for brevity): the system is able to track all setpoints, both in terms of position and orientation. In Fig. 7a it can be noted that the thrust of UAV 1 seems to be of consistently larger magnitude than that of UAV 2, which is inline with the non-symmetric placement of the bars CoM discussed in Section VI.

B. Decentralized MPC

Fig. 6c shows position of all rigid bodies, as well as the reference signals (in dashed lines); however, as the bar centerpoint was no longer being tracked, its estimated position was calculated as $\boldsymbol{p}_b = \boldsymbol{p}_p^{(1)} + 2^{-1}(d_1 + d_2)(\boldsymbol{p}_p^{(2)} - \boldsymbol{p}_p^{(1)})$. Fig. 6d shows the orientations of the UAVs, as well as the estimated yaw angle of the bar, calculated by $\arctan2(y_p^{(2)} - y_p^{(1)}, x_p^{(2)} - x_p^{(1)})$, where $x_p^{(i)}$, $y_p^{(i)}$ are the x and y positions of payload i, and $\arctan2 : \mathbb{R}^2 \to (-\pi, \pi]$ is the function commonly found in many programming languages which, in contrast to $\arctan$, returns values in the range $(-\pi, \pi]$. Figs. 7c and 7d show the resulting optimal control signals, where it should be noted that the relatively large difference between the thrust signals of UAV 1 and 2 likely stems from the differences in $m_p^{(i)}$ (eq. (13)) as discussed in Section VI.

C. Comparison

Fig. 8 shows errors and magnitudes that will aid in the comparison: Fig. 8a the L^2-norm of UAV 1's error in position (top) and orientation (bottom); Fig. 8b the thrust magnitude (top) and the L^2-norm of the torques; Fig. 8c the absolute error in all three dimensions of the bar centerpoint position (top) and the error in yaw orientation (bottom). Starting with Fig. 8a, we notice that the position errors of the UAV are close to identical. In the case of the orientation, the decentralized setup achieves a faster convergence time, which is likely a result of the difference in tuning. The results in Fig. 8b do not indicate any clear differences between the two setups, apart from the temporary increase in torque magnitude for the centralized setup occurring between sec. 10–15. Since this event coincides with UAV 1 being rotated $-90°$, this could eventually be caused by a failure to attach the cables to the UAV CoM, thereby introducing rotational forces not part of the system model. The noise-affected appearance of the input signals could be attributed to that: i) the velocity estimate is noisy; ii) the transfer of the input from the MPC to the vehicle is sub-optimal, resulting in overshoots that the MPC has to compensate for. Fig. 8c, in contrast, displays a notable difference between the two setups: in the decentralized (dashed) case, the position and yaw angle error seem to have a more oscillatory character, and the yaw error convergence between sec. 27–35, is slower. To quantify this we use the error in the x-position as a proxy, and calculate the arithmetic mean and sample standard deviation for the two cases. Note that perfect tracking would be equivalent to both these quantities being zero. Results are given in Table III and give the decentralized MPC a mean approximately four times further away from zero, and a two times higher standard deviation compared to the centralized MPC. Another important comparison factor is the CPU time: during the experiments a time average of 2.8 ms, and 7.0 ms is achieved for the decentralized and centralized case, respectively. The decentralized MPC was thus found to have a 2.5 times faster execution time.

TABLE III: Statistics of the error in bar centerpoint x-position.

	Mean	Std. dev.
Centralized MPC	–0.055 14 m	0.058 46 m
Decentralized MPC	0.234 68 m	0.125 54 m

A conclusion can then be drawn: a centralized approach where the dynamics of the bar are incorporated results in better tracking of the bar, but comes at the cost of increased computational time and lack of redundancy. However, there are also characteristics, inherent to each setup, that should be considered in the choice between a centralized and a decentralized setup. By decentralizing the control problem, a higher resilience towards system failure is achieved, since the failure of one agent does not necessarily mean the failure of the rest. Possibly, the closed-loop performance of the decentralized setup could be improved by incorporating more feedback into the model. As an example, the relative distance between UAVs could be tracked and fed into the controller.

VIII. CONCLUSIONS AND FUTURE WORK

The aim of this work was to investigate the effectiveness and performance of model predictive controllers when applied to the case of collaborative payload transport using UAVs. For this purpose, two different MPCs were proposed and designed: a centralized, and a decentralized. Both con-

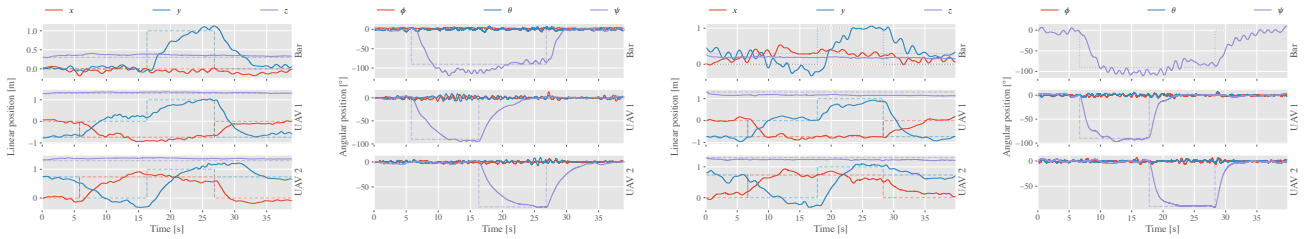

(a) (b) (c) (d)

Fig. 6: Experimental results showing position and orientation of both UAVs and bar for the: (a), (b) centralized MPC; (c), (d) decentralized MPC. Dashed lines denote the reference signal.

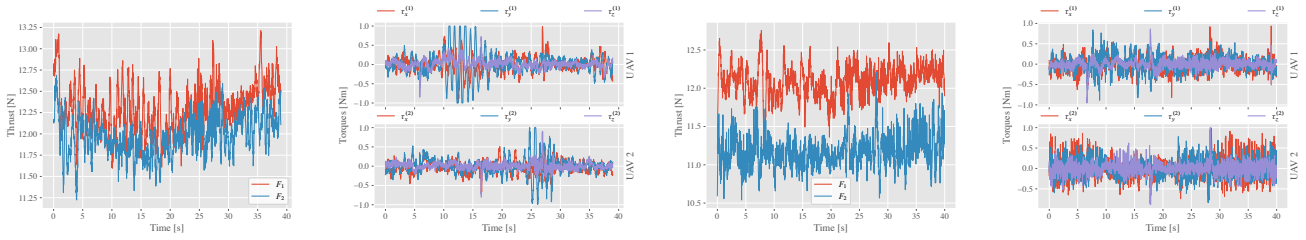

(a) (b) (c) (d)

Fig. 7: Experimental results showing thrust and torques of both UAVs for the: (a), (b) centralized MPC; (c), (d) decentralized MPC.

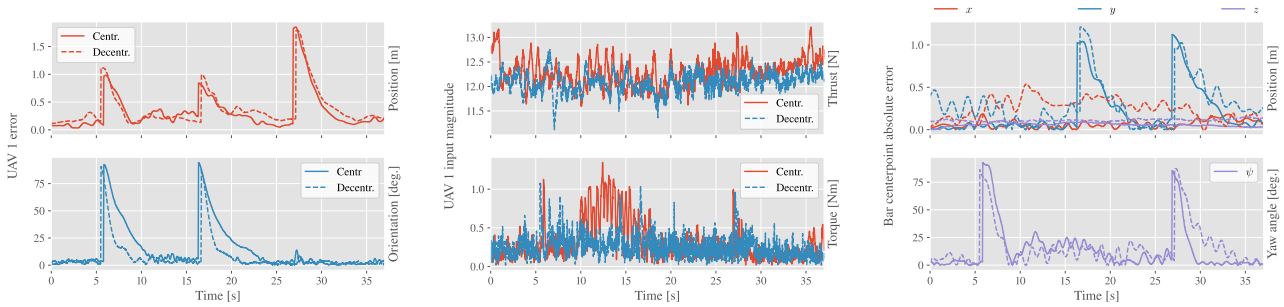

(a) (b) (c)

Fig. 8: Plots showing the experimental results in terms of: (a) UAV 1 error; (b) input magnitude; (c) bar error. Dashed lines denote results from the decentralized setup.

trollers were set up on an experimental platform where they successfully were able to track a number of setpoints. The centralized MPC gave better tracking of the bar, but had a higher CPU time than the decentralized. Both controllers seemed to perform equally in terms of UAV tracking.

This work demonstrated that MPC can be utilized to successfully control a UAV–bar system. Future work includes the consideration of imperfect state estimation, as well as systems with more UAVs and more complicated payload geometries. Although a decentralized attempt was done in this work, the performance could likely be improved by further investigation into *e.g.*, if there are any quantities that should be transmitted between agents, and/or looking at if it is possible to incorporate more of the dynamics caused by the cable tension without adding to the model complexity.

References

[1] J. Qi, D. Song, H. Shang, N. Wang, C. Hua, C. Wu, X. Qi, and J. Han, "Search and rescue rotary-wing UAV and its application to the lushan ms 7.0 earthquake," *Journal of Field Robotics*, vol. 33, no. 3, pp. 290–321, jul 2015.

[2] X. Li, Q. Yang, Z. Chen, X. Luo, and W. Yan, "Visible defects detection based on UAV-based inspection in large-scale photovoltaic systems," *IET Renewable Power Generation*, vol. 11, no. 10, pp. 1234–1244, jun 2017.

[3] N. Metni and T. Hamel, "A UAV for bridge inspection: Visual servoing control law with orientation limits," *Automation in Construction*, vol. 17, no. 1, pp. 3–10, nov 2007.

[4] D. Roca, S. Lagüela, L. Díaz-Vilariño, J. Armesto, and P. Arias, "Low-cost aerial unit for outdoor inspection of building façades," *Automation in Construction*, vol. 36, pp. 128–135, dec 2013.

[5] G. Tartaglione, E. D'Amato, M. Ariola, P. S. Rossi, and T. A. Johansen, "Model predictive control for a multi-body slung-load system," *Robotics and Autonomous Systems*, vol. 92, pp. 1–11, jun 2017.

[6] M. Gassner, T. Cieslewski, and D. Scaramuzza, "Dynamic collaboration without communication: Vision-based cable-suspended load transport with two quadrotors," in *2017 IEEE International Conference on Robotics and Automation (ICRA)*. IEEE, may 2017.

[7] T. Lee, "Geometric control of quadrotor UAVs transporting a cable-suspended rigid body," *IEEE Transactions on Control Systems Technology*, vol. 26, no. 1, pp. 255–264, jan 2018.

[8] P. O. Pereira and D. V. Dimarogonas, "Collaborative transportation of a bar by two aerial vehicles with attitude inner loop and experimental validation," in *2017 IEEE 56th Annual Conference on Decision and Control (CDC)*. IEEE, 12 2017, pp. 1815–1820.

[9] B. E. Jackson, T. A. Howell, K. Shah, M. Schwager, and Z. Manchester, "Scalable cooperative transport of cable-suspended loads with

UAVs using distributed trajectory optimization," *IEEE Robotics and Automation Letters*, vol. 5, no. 2, pp. 3368–3374, apr 2020.

[10] C. Gabellieri, M. Tognon, D. Sanalitro, L. Pallottino, and A. Franchi, "A study on force-based collaboration in swarms," *Swarm Intelligence*, vol. 14, no. 1, pp. 57–82, nov 2019.

[11] J. Wehbeh, S. Rahman, and I. Sharf, "Distributed model predictive control for UAVs collaborative payload transport," in *2020 IEEE/RSJ International Conference on Intelligent Robots and Systems (IROS)*. IEEE, oct 2020.

[12] R. Mahony, V. Kumar, and P. Corke, "Multirotor aerial vehicles: Modeling, estimation, and control of quadrotor," *IEEE Robotics & Automation Magazine*, vol. 19, no. 3, pp. 20–32, sep 2012.

[13] T. Lee, M. Leok, and N. H. McClamroch, "Geometric tracking control of a quadrotor UAV on SE(3)," in *49th IEEE Conference on Decision and Control (CDC)*. IEEE, dec 2010.

[14] P. Pereira, J. Cortes, and D. V. Dimarogonas, "Aerial slung-load position tracking under unknown wind forces," *IEEE Transactions on Automatic Control*, vol. 66, no. 9, pp. 3952–3968, Sep. 2021.

[15] B. Siciliano and O. Khatib, Eds., *Springer Handbook of Robotics*, 2nd ed. Springer International Publishing, 2016.

[16] P. O. Pereira and D. V. Dimarogonas, "Pose stabilization of a bar tethered to two aerial vehicles," *Automatica*, vol. 112, p. 108695, Feb. 2020.

[17] J. A. E. Andersson, J. Gillis, G. Horn, J. B. Rawlings, and M. Diehl, "CasADi: a software framework for nonlinear optimization and optimal control," *Mathematical Programming Computation*, vol. 11, no. 1, pp. 1–36, jul 2018.